Pharm Res (2012) 29:1495–1505
DOI 10.1007/s11095-011-0624-1

RESEARCH PAPER

# Transferrin Adsorption onto PLGA Nanoparticles Governs Their Interaction with Biological Systems from Blood Circulation to Brain Cancer Cells

Jiang Chang • Archibald Paillard • Catherine Passirani • Marie Morille • Jean-Pierre Benoit • Didier Betbeder • Emmanuel Garcion

Received: 3 September 2011 / Accepted: 31 October 2011 / Published online: 14 December 2011
© Springer Science+Business Media, LLC 2011

## ABSTRACT

***Purpose*** Nanomedicines represent an alternative for the treatment of aggressive glioblastoma tumors. Behaviour of PLGA-nanoparticles (NPs) was here investigated as a function of their protein adsorption characteristics at the different biological interfaces they are expected to face in order to reach brain cancer cells.

***Methods*** NPs were studied for size, zeta potential, blood half-life, *in vitro* endocytic behavior and *in vivo* accumulation within healthy rat brain and brain tumors.

***Results*** While slightly modifying size (80 to 90 nm) and zeta potential (−44 to −32 mV) protein coating of PLGA-NPs by bovine serum albumin (BSA) or transferrin (Tf) greatly prolonged their blood half-life when intravenously injected in rats and mice. In contrast with THP-1 monocytes, differentiated THP-1 macrophages, F98 glioma cells and astrocytes internalized BSA- and Tf-NPs *in vitro*. Increase of Tf-NP uptake by F98 cells through caveolae- and clathrin-mediated pathways supports specific interaction between Tf and over-expressed Tf-receptor. Finally, *in vivo* targeting of healthy brain was found higher with Tf-NPs than with BSA-NPs while both NPs entered massively within brain-developed tumors.

***Conclusion*** Taken together, those data evidence that Tf-NPs represent an interesting nanomedicine to deliver anticancer drugs to glioma cells through systemic or locoregional strategies at early and late tumor stages.

**KEY WORDS** blood–brain barrier · central nervous system · glioma · PLGA nanocarriers · stealth · targeting

## INTRODUCTION

Glioblastoma are extremely aggressive tumors of the central nervous system (CNS). Although their incidence is increasing, the standard treatment, combining surgical removal when possible with external radiotherapy, has remained almost unchanged during the last thirty years (1). This stagnation in therapeutic approach is partly due to the high resistance of glioblastoma cells, but also to an inefficient delivery of drugs. Hence, eradication of infiltrating tumour cells within the CNS represents a major objective but faces two substantial difficulties: the vulnerability of the neural tissue, and the relative impermeability of the blood–brain barrier (BBB). In addition, the escalation of intravenous drug doses is restricted by a rapid increase in their systemic toxicity.

Among alternatives, drug delivery nanosystems derived from nanotechnologies are perhaps the most relevant and potentially useful in this biological context (2). Liposomes (3–7), polymer nanospheres (8), polymer nanocapsules (9), lipid nanocapsules (10–15) or nanoemulsions (16), can either be implanted within the tumor

J. Chang and A. Paillard contributed equally to this work.

J. Chang • D. Betbeder
EA 4483, Laboratoire de physiologie
Université de Lille 2
Lille, France

J. Chang • D. Betbeder
Université d'Artois
Arras, France

A. Paillard • C. Passirani • M. Morille • J.-P. Benoit • E. Garcion
LUNAM Université, Université d'Angers
Ingénierie de la Vectorisation Particulaire
Angers, France

A. Paillard • C. Passirani • M. Morille • J.-P. Benoit • E. Garcion
INSERM, U646
Angers, France

or within the resection cavity or instead, delivered via the blood to the CNS tumor site. Nano-objects can indeed travel in biological media from which they interact with a wide range of molecules and systems (11,17–20). From infusion sites (21,22) to intracellular targets (23,24), they may offer new opportunities to tackle a succession of biological obstacles (25). Drugs encapsulated in NPs can thus present a better solubility, with improved biological barrier crossing properties and better controlled release kinetics, leading to substantial clinical advantages including dose reduction, prevention of side effects and improvement of bioavailability within the targeted tumor cell (2,26,27).

With respect to the crossing of the BBB, only a few studies have demonstrated the potential value of nanocarriers. These include the use of poly(d,l-lactide-co-glycolide) (PLGA) (28), maltodextrin (29–31) and poly (cyanoacrylate) (32,33) nanoparticles. In parallel, research on the identification of specific receptors on the surface of brain capillary epithelium has constituted the basis for further studies on the coating of nanoparticles with functional ligands to facilitate specific BBB crossing. As such, receptor mediated transcytosis was identified for LDL (34), insulin (35) or transferrin (Tf) (36). Targeted drug delivery through the Tf receptor (TfR) pathway has received special attention with the use of Tf itself or one of the antibodies directed against the TfR (37). Several synthetic or biomimetic nanoparticles were developed for this purpose including polyethyleneglycol polycyanoacrylate (38), cationic lipid magnetic (39), PLGA (40), lipoplexes (41,42), polymer-based cyclodextrin (43), and gold nanoparticles (44) as well as lipid immunonanocapsules (45).

Among those, PLGA-nanoparticles (NPs) offer the advantage of being made from biocompatible and biodegradable components that do not induce inflammation or immune reactions (46) and, thus, of being approved by the US Food and Drug Administration (FDA). As such, we recently developed 90 nm NPs free from toxic surfactant that were combined with Tf (47). Those new nanocarriers differ from previously developed Tf-NPs (40,48–50) as a result of: i) non-covalent grafting of Tf with no constraint of organic solvent which could have affected the Tf-binding capability and/or the activity of therapeutic molecules further loaded within the PLGA matrix, and ii) smaller size that is an important parameter for their diffusion to the brain (47). Thus, they were studied for brain endothelial cell targeting (47) as well as blood–brain barrier crossing (51) demonstrating their potential for active targeting of brain tissue.

The aim of the present study was to investigate the behaviour of NPs when confronted with the various biological hurdles they are expected to encounter on their pathway to the target brain cancer cells. Three types of NPs were studied as a function of their protein adsorption characteristics: native blank-NPs, control BSA-NPs or Tf-NPs that allow specific targeting of cells expressing Tf receptor. The relevance of these nanocarriers for further preclinical or clinical studies involving systemic or brain locoregional active targeting is further discussed in the light of the data presented.

## MATERIALS AND METHODS

### Materials

PLGA (50:50, Resomer® RG 503H; Mw = 26,500 g/mol; Mn = 14,700 g/mol) was purchased from Boehringer Ingelheim (Germany). Fluorescent dye 1,1′-dioctadecyl 3′3,3′,3′-tetramethylindo-carboxycyanate perchlorate (DiI), bovine serum albumin (BSA), bovine serum albumin-FITC conjugate and human *holo*-Tf (≥ 98%) were from Sigma Chemical Co. (Saint Louis, MO). Sephadex G25 column (PD 10) was purchased from Amersham (Orsay, France). Phosphate-buffered saline (PBS) was composed of 150 mM NaCl, 2.7 m*M* KCl, 1.3 m*M* $KH_2PO_4$ and 1 mM $Na_2HPO_4.7H_2O$, pH = 7.4; bicarbonate buffer 0.1 M pH = 9.5 was obtained by mixing a $NaHCO_3$ solution at 0.1 M with a $Na_2CO_3$ at 0.1 M to obtain a final solution at pH = 9.5. The *Etablissement Français du Sang* (Angers, France) provided the Normal human serum (NHS) and Biomérieux (Sérum hémolytique, Biomérieux, France) supplied the rabbit anti-sheep erythrocyte antibodies. Chlorpromazine, nystatin, phorbol 12-myristate 13-acetate (PMA), 5-(N,N-dimethyl) amiloride hydrochloride (DMA) were from Sigma-Aldrich (Saint Quentin Fallavier, France).

### Preparation of Nanoparticles

Blank NPs were obtained by a modified solvent diffusion (nanoprecipitation) technique (Barichello *et al.*, 1999). Briefly, PLGA (10 mg) was solubilized in acetone (850 µL), and then 150 µL ethanol (97%) was added. This organic phase was quickly poured into 10 mL deionized water (aqueous phase) under magnetic stirring at 1000 rpm for 3 h. Fluorescent NPs were prepared using the same

E. Garcion (✉)
Inserm U646, IBS – CHU Angers
4 rue Larrey
49933 Angers cedex 9, France
e-mail: emmanuel.garcion@univ-angers.fr

D. Betbeder (✉)
EA 4483, Faculté de Médecine Pôle Recherche
Laboratoire de Physiologie
1 place de Verdun
59000 Lille, France
e-mail: dbetbeder@aol.com

procedure, and DiI was added to the acetone solution of PLGA. The suspensions were then kept at 4°C and sterilized by filtration through 0.22-μm filters.

Protein (human *holo*-Tf or bovine serum albumin) was dissolved in Ringer-Hepes buffer (RH, pH=7.4) at a concentration of 1 mg/mL. Blank NPs were added to the protein solutions at a ratio of 1/1 (w/w). The adsorption reaction was left for 3 h at room temperature, with moderate shaking (Ataman-Onal *et al.*, 2006). The protein-NPs were ultra-filtered by 100 kDa "Millipore" (Amicon Centriplus 100 K MWCO) to eliminate free BSA or Tf. Final protein-NP concentration in NaCl physiologic serum was 1 mg/mL.

### Size and Zeta Potential Determination

The particle size and size distribution of NPs were measured by using a N4 PLUS submicron particle size analyzer (Beckman Coulter, N4 Plus software). Before measurement, the particle suspension was diluted with PBS (pH=7.4). The samples were examined for their mean particle diameter and polydispersity. The reported values are mean ± s.d. (n=3). Particle size stability at 4°C or 37°C was evaluated in sterile water (1 mg/mL of these NPs) at different time intervals. NP surface charge was investigated through zeta potential measurements in 15 mM NaCl (Zetasizer 4, with a multi-8 correlator 7032, Malvern Instruments).

### Transmission Electron Microscopy (TEM) of nanoparticles

The NPs were examined by transmission electron microscopy (TEM) following negative staining with sodium phosphotungstate solution (0.2%, w/v) (52). A drop of the sample was placed onto a carbon-coated copper grid to create a thin film. Before the film dried on the grid, it was negatively stained with phosphotungstic acid by adding a drop of the staining solution to the film; any excess solution was drained off using a filter paper. The grid was allowed to dry, and samples were viewed under a transmission electron microscope (JEOL-100CX-II, Tokyo, Japan).

### Determination of the *In Vivo* Plasma Circulation Time

Swiss mice and Fisher rats were obtained from the Charles River Laboratory. Animal care was carried out in strict accordance to French Ministry of Agriculture regulations. The animals were kept in standard animal facilities with free access to food and water. They were housed in a temperature and humidity-controlled room with a 12 h on-off light cycle and were put down at the end of each experiment. Mice and rats were anesthetized with isofluran (3%+$O_2$) and injected intravenously in the tail vein (200 μg of DiI labeled NPs/mouse, $n \geq 3$, or 500 μg of DiI labeled NPs/rats, $n \geq 3$). Blood samples (0.5 ml) were withdrawn by orbital sinus or endocardiac blood collection at 1, 5, 15, 30, 60 and 120 min after injection. Serum was measured at $\lambda_{ex}=544$ nm and $\lambda_{em}=590$ nm with a Spectro-fluorometer Fluoroskan Ascent Fl (Thermo Labsystems).

### *In Vitro* NP Uptake by Undifferentiated and Differentiated Monocyte/Macrophage THP-1 Cells

THP-1 cells (human monocyte/macrophage cell line obtained by ATCC, Manassas, VA, USA) were grown in suspension in a humidifier-incubator (5% $CO_2$) at 37°C in ATCC suggested medium. THP-1 differentiation was obtained by addition of 200 nM Phorbol 12-myristate 13-acetate (PMA, Sigma, Saint-Quentin Fallavier, France) for 24 h to allow adherence and differentiation (53). Undifferentiated THP-1 monocytes or differenciated THP-1 macrophages were incubated in 24-well plates in the presence of BSA- or Tf-NPs at 100 μg/mL, 50 μg/mL, 25 μg/mL, 10 μg/mL in serum-containing culture medium for 2 h at 37°C. NP endocytosis was analyzed by flow cytometry as previously described (11), with 10000 cells measured in each sample on a BD FACSCalibur™ fluorescent-activated flow cytometer using the BD CellQuest™ software (BD-Biosciences).

### Glioma and Newborn Rat Primary Astrocyte Cultures

F98 glioma cells were obtained from ATCC (CRL-2397, American Type Culture Collection, Manassas, VA, USA). They were grown at 5% $CO_2$ and 37°C in Dulbecco modified Eagle medium (DMEM) containing glucose and L-glutamine (Bio Whittaker, Verviers, Belgium), and added with 10% foetal bovine serum (FBS, Biowhittaker) and 1% antibiotic and antimycotic solution (Sigma, Saint-Quentin Fallavier, France). Purified newborn rat primary astrocytes were obtained by the mechanical dissociation method from cultures of cerebral cortex as originally described (54). They were grown at 37°C/5% $CO_2$ in DMEM with glucose and l-glutamine containing 10% FBS (Bio Whittaker) and 1% antibiotic and antimycotic solution (Sigma).

### *In Vitro* NP Uptake by F98 Glioma Cells and Astrocytes

#### *Flow Cytometry Analysis*

DiI-labeled BSA- or Tf-NPs were incubated either at 50 μg/ml, or at concentrations indicated in the figure legends, with glioma cells or astrocytes in serum-free medium for 2 h before flow cytometry analysis performed as described above.

### *Cell Treatment with Chemical Inhibitors of Known Endocytic Pathways*

Previously identified chemical inhibitors of known endocytic pathways were used as described elsewhere (55). Briefly, glioma cells were pre-treated with inhibitors for 1 h at 37°C in serum-free culture medium. Depletion in cholesterol was carried out by use of methyl-β-cyclodextrin (MβCD) in the presence of lovastatin (56). Chlorpromazine and potassium depletion (57) were used to inhibit clathrin-mediated transport, while PMA was used to selectively disrupt caveolae and DMA to inhibit macropinocytosis (58).

### *Immunofluorescence Combined Flow Cytometry to Assess Plasma Membrane TfR Expression*

Glioma cells or astrocytes were scrapped, washed twice in PBS and resuspended in PBS containing 5% FBS and 0.02% NaN3 before incubation at 4°C for 1 h with 5 µg/mL IgG2a isotype control immunoglobulins (BD-Biosciences) or 5 µg/mL OX26 monoclonal antibody (Abcam, Cambridge, UK) recognizing the TfR. After extensive washing, the cells were further stained for 30 min at 4°C with FITC-conjugated goat anti-mouse IgG F(ab')2 fragment polyclonal antibody (Dakocytomation, Trappes, France) at 20 µg/mL in PBS containing 5% FBS and 0.02% sodium azide. Following three more washes in PBS containing 5% FBS and 0.02% sodium azide, cells were re-suspended in PBS containing 2% formaldehyde and 0.02% sodium azide andanalysed by flow cytometry as described above.

## *In Vivo* Tumour Model to Address the Intracerebral Distribution of DiI-labeled NPs

Twenty-four syngeneic F344 Fischer female rats (Charles River, Cléon, France) weighing 150 to 200 g were used for this study. They were kept in standard animal facilities with free access to food and water. All experiments were conducted under good experimental practices according to regulations of the European Commission and the French Ministry of Agriculture. For tumour induction, F98 glioma cells were trypsinised by trypsine/EDTA (Sigma), washed and resuspended at $5.10^2$ cells in 10 µl Eagle minimum essential medium (Biowhittaker) before surgical stereotaxic implantation. Rats were anaesthetised intraperitoneally with 10 mg/kg xylazine (Rompun) and 50 mg/kg ketamine (Clorketam) before being placed in a Kopf stereotaxic frame (Harvard Apparatus, Les Ulis, France). After shaving, disinfection and sagittal incision of the cranial skin, a burr hole was made in the skull at 0.5 mm anterior and 3 mm lateral from the Bregma using a small drill. Suspensions were then injected at 5 mm below the dura in the right striatum according to the Paxinos atlas. The needle was afterwards removed cautiously before the wound was sutured. For studying the accumulation of DiI-labeled NPs within the brain, animals were anesthesized under isoflurane and injected i.v.(caudal vein) with either vehicle alone, Dil-BSA- or Dil-Tf-NPs at 2 µg/g of bodyweight. To study NP accumulation within brain tumors, i.v.-injections were performed at day 19 after F98 cell implantation, when tumors were largely established and clearly detectable through MRI (magnetic resonance imaging). Evaluation of DiI fluorescence within the brain was made at 2 and 24 h after i.v.-injections for healthy animals and at 24 h for brain tumor accumulation. All rats were killed by $CO_2$ inhalation. The brains were surgically removed, snap-frozen in liquid nitrogen-chilled isopentane and stored at −80°C. Frontal cryosections (14 µm) were performed at about 0.5 mm anterior from the Bregma using a Cryocut 3000 (Leica, Rueil-Malmaison, France). The resulting slides were kept at −20°C before processing. They were then allowed to dry for 30 min at room temperature, fixed at 4°C in 4% paraformaldehyde in PBS for 10 min. Finally, they were washed 3 times with PBS before mounting in 1/1 (v/v) PBS/Dako Cytomation fluorescent mounting medium (Trappes, France). Two slides per animal were included in the analysis on which three images were randomly collected: i) at the external edge of the right cerebral hemisphere (cortex) in an area ranging from 1 to 3 mm lateral from Bregma and 1 to 2 mm below dura for brain accumulation of DiI after i.v.-injections of DiI-NPs in healthy animals, and ii) at the center of the developed tumor for accumulation of DiI after i.v.-injections of DiI-NPs in orthotopic F98 tumor bearing rats. All slides were examined under an Axioskop-2 Zeiss fluorescence micro-

**Table I** Mean Diameters (nm), Polydispersity Index (PI) and Zeta Potential of PLGA NPs (mV) (*$p < 0.05$; Data as Mean ± s.d.; $n = 3$)

| Samples | Particle size | | Zeta potential (mV) |
|---|---|---|---|
| | Mean diameter (nm) | p.i | |
| Blank NPs | 63.3 ± 23.6 | 0.037 | −42.6 ± 6.6 |
| Dil labeled Blank-NPs | 79.2 ± 25.3 | 0.029 | −44.2 ± 8.9 |
| Dil labeled BSA-NPs | 90.2 ± 26.8 | 0.132 | −33.1 ± 7.7* |
| Dil labeled Tf-NPs | 88.8 ± 27.5 | 0.176 | −32.5 ± 8.2* |

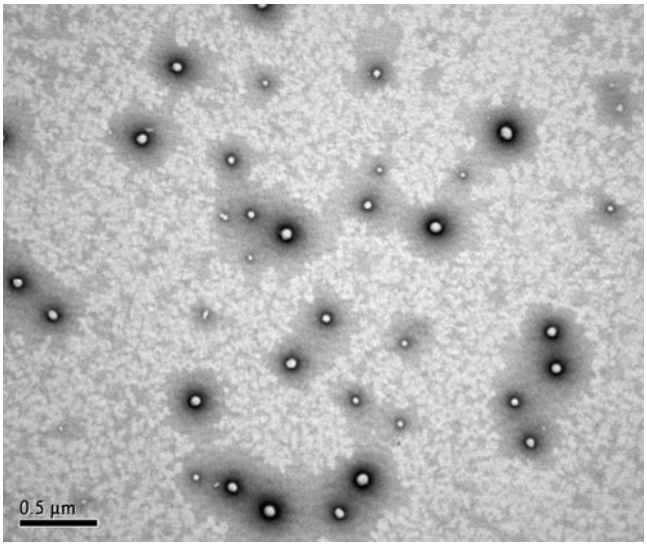


**Fig. 1** Transmission electronic microscopy images of Blank NPs after negative staining. Bar represents 0.5 $\mu$m.

scope (Le Peck, France). Images were acquired through a Photometrics CoolSNAP ES camera equipped with a QImaging CRI Micro Color 2 RGB Liquid Crystal filter and by using the MetaVue™ imaging system (all from Roper Scientific, Evry, France). Images analysis was performed via integrated morphometry after inclusive thresholding by use of the Metamorph ® software (Roper Scientific).

### Statistical Analysis

XLSTAT 2006 Version 2006.3 (Addinsoft Paris, France) was used for statistical analyses. Statistical significance for each experiment was determined by a Dunnett's test and by a Fisher's test. The tests were considered as significant with p values of less than 0.05 or 0.01.

## RESULTS AND DISCUSSION

### Nanoparticle Characterization

NPs were prepared using the solvent diffusion technique. Size distribution of all particles was unimodal with a mean diameter of 63 to 90 nm (Table I). Transmission electron microscopy showed that the NPs were almost spherical in shape (Fig. 1). DiI incorporation in blank-NPs increased their mean hydrodynamic diameter from 63 nm to 79 nm. Furthermore, as expected, a further increase in size was

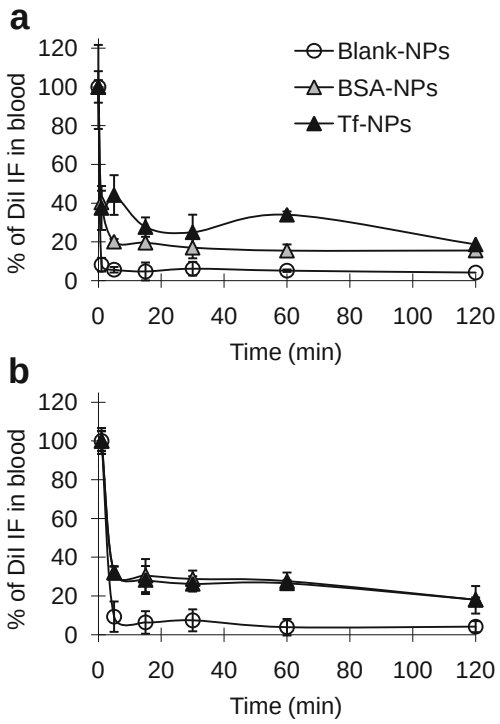


**Fig. 2** Plasmatic concentration-time profiles of NPs labeled with DiI, after intravenous injection in mice (**a**) and in rats (**b**). Results are expressed as% of injected dose. BSA-NPs (Δ), Tf-NPs (▲). Data represented mean ± s.e.m. of a triplicate obtained from one representative experiment that was reproduced twice.

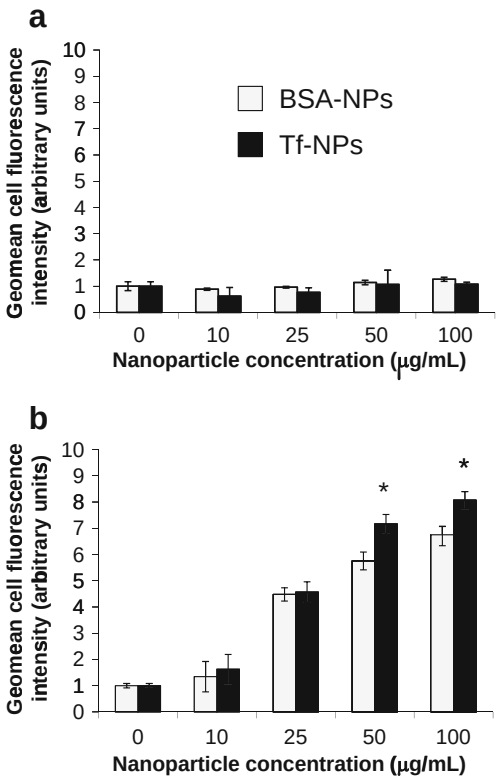


**Fig. 3** NP uptake by THP-1 like monocytes (**a**) or macrophages (**b**) depending on concentration. Dunnett's test: $*p < 0.05$. Data represented mean ± s.e.m. of a triplicate obtained from one representative experiment that was reproduced twice.

observed when proteins were adsorbed on their surface. Protein loading was estimated to be about 126 μg of BSA (1.89 nmole) and 89 μg of Tf (1.11 nmole) per mg of NPs as previously established (47). The zeta potential of Blank NPs increased when BSA or Tf was adsorbed on the NPs, while DiI labeling did not affect their zeta potential (Table I). Short-term size stability of the particles over time was evaluated at 4°C and 37°C (data not shown). No size increase was observed at 4°C after 28 days storage, while at 37°C only Blank NPs slowly aggregated after 8 days incubation confirming that Blank NPs prepared without surfactant were colloidaly unstable and rapidly coalesced (59).

We followed the stability of protein adsorption on NPs at 37°C. No protein desorption was observed even after 12 days incubation (47). To quantify the endocytosis of NPs by the endothelial cells, we used the fluorescent dye DiI as a lipophile marker. No change of fluorescence intensity of NPs after 1-week incubation at 37°C suggested high DiI stability. To further confirm this result, NPs were centrifuged at 13,000 × g for 30 min and NPs were then recovered in suspension and passed through 0.22-μm filter. No DiI was lost during this process, contrary to free DiI, which could not be filtered confirming DiI incorporation in NPs.

## Nanoparticle Behavior with Blood Elements

When injected through the systemic pathway, PLGA-NPs will be confronted with blood components and processes that include opsonin adsorption, activation of the complement system, phagocytosis by monocyte/macrophage cells and, overall, removal by the reticulo-endothelial system (60,61). Properties currently known to affect clearance include particle components, size, shape, porosity, surface chemistry and surface charge (62). Thus, we initially study plasma circulation time of Blank-, BSA and Tf-NPs. As evidenced in the mouse and rat model (Fig. 2a and b, respectively), the Blank-NPs have the shortest half-life, proof that the protein surface coating prevented interactions between the serum and the NPs, which could lead to

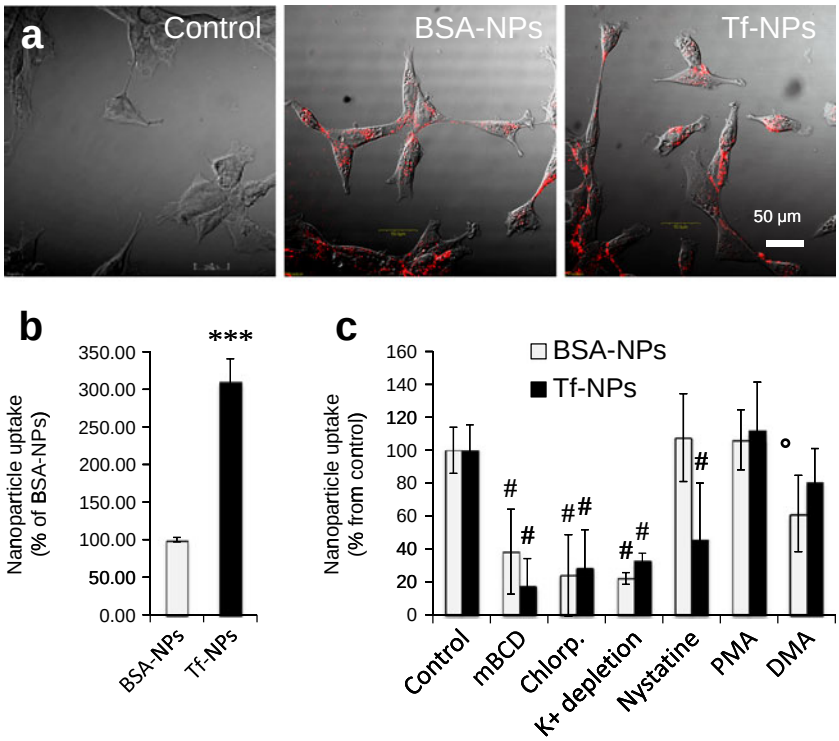


**Fig. 4** Confocal analysis of NP interaction with glioma cells. (**a**) NP localization in F98 cells after 2 h of incubation at 37°C. Control represents cells that were not incubated with NPs. (**b**) Relative NP uptake by F98 cells after 2 h incubation with DiI-NPs at 37°C depending on protein adsorption. Data showed one representative experiment that was reproduced three times with quantifications representing the variation in% from the BSA-NPs condition of geomean fluorescence intensity per single cell calculated on 10 000 events for each samples repeated in triplicates. (**c**) Mechanisms involved in active endocytosis of DiI-NPs assessed by the variation of the basal mean fluorescence intensity of F98 cells after 2 h incubation at 37°C after treatment with known inhibitors of endocytosis pathways. Data showed one representative experiment that was reproduced three times with quantifications representing the variation in% from either the BSA-NPs or the Tf-NPs condition of geomean fluorescence intensity per single cell calculated on 10 000 events for each samples repeated in triplicates. mBCD: treatment with methyl-β-cyclodextrine combined with lovastatine. Chlorp.: chlorpromazine treatment. K+ depletion: depletion in potassium. Dunnett's test: $^{***}p < 0.001$, differences between BSA- and Tf-NPs; $^{\#}p < 0.001$ and $^{\circ}p < 0.05$, differences from control.

eventual elimination of the vector from blood. Higher blood clearance of Blank NPs might be due to the NP aggregation in serum and also to their lipophilic surface, which is known to induce opsonisation and uptake by the mononuclear phagocyte system. Protein coated PLGA-NPs had higher blood circulation time for the first 2 h after i.v. injection compared to Blank-NPs that were almost totally eliminated within minutes after i.v. injection. In order to reach the brain, this stealth property is a prerequisite.

### Effect of Protein Adsorption on the NP Behavior on Monocytes and Macrophages

Having established that Blank-NPs were non-circulating, those native NPs were no longer studied in contrast to BSA- and Tf-NPs that were further analyzed for their interaction with reticulo-endothelial constituent cells. Figure 3 illustrates the interactions of PLGA-NPs with non-differentiated and non-adhesive human THP-1 cells, which mimic circulating monocytes (Fig. 3a), and the differentiated and adhesive THP-1 cells which correspond to the resident macrophages (Fig. 3b). The important point to be noted is that for all the NPs tested, there was no visualized interaction with monocytes (Fig. 3a) in contrast to macrophages (Fig. 3b), thus emphasizing low phagocytic capability of undifferentiated THP-1 monocytes (63). Interestingly, NP uptake by differentiated THP-1 cells was observed from the dose of 25 µg/mL (Fig. 3b). Significant differences were observed between Tf-NPs and BSA-NPs. This data could be explained by expression of the Tf-receptor at the surface of THP-1 cells. As such, distinct accessibility to the Tf-receptor at the cell surface of monocytes and transformed macrophages have been described as a result of low Tf-receptor expression on monocytes as compared to mature macrophages (64) and/or molecular changes in plasma membrane domains ascribed to endocytosis (65). As the Tf-receptor in THP-1 cells is excluded from caveolae (65), clathrin-dependent receptor-mediated endocytosis might be a basal mechanism for the uptake of Tf-NPs in those cells (37,66), while not excluding non-specific endocytosis such as fluid phase macropinocytosis.

### Effect of Protein Adsorption on the NP Behavior on F98 Glioma Cells and Astrocytes

In the case of anti-glioblastoma treatment, many drugs need to be delivered intra-cellularly to exert their function inside the cytoplasm, the nucleus or specific organelles. Thus, the behavior of PLGA-NPs requires careful evaluation in targeted glioma cells notably with regard to plasma membrane crossing by endocytosis and drug delivery to the cytosol in order to reach extra-endolysosomal targets.

As shown in Figs. 4a and b, both BSA- and Tf-NPs were internalized by F98 cells. As indicated by semi-quantitative flow cytometry analysis, Tf-NPs showed higher uptake by glioma cells compared with BSA-NPs, thus indicating that Tf conferred specific features for endocytosis within glioma cells (Fig. 4b). To understand which mechanism was implied, the involvement of specific pathways of endocytosis was studied by using previously identified chemical inhibitors of known endocytosis pathways. The results presented in Fig. 4c further corroborate the assumption that it is the surface coating which influences NP uptake by F98 cells. We found that Tf-NPs are endocytosed via caveolae- and clathrin-

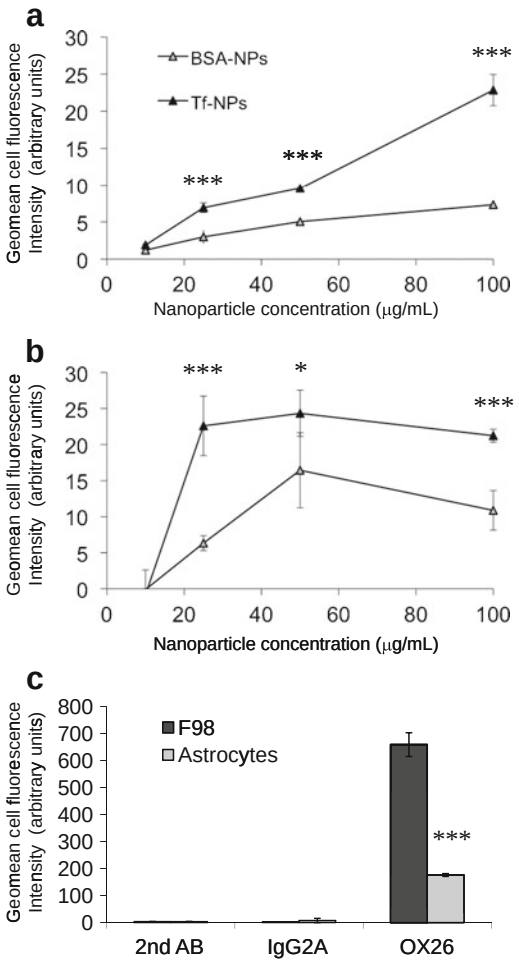


**Fig. 5** Dose–response uptake analysis performed at increasing concentrations of DiI-NPs after 2 h incubation at 37°C in F98 glioma cells (**a**) or astrocytes (**b**). (**c**) Evaluation of Tf-receptor expression by flow cytometry using the OX26 antibody on F98 cells and astrocytes. 2ndAB: control with secondary antibody tested alone. IgG2A: control with IgG2a immunoglobulins instead of OX26 antibody. Data showing one representative experiment that was reproduced three times are expressed as geomean fluorescence intensity per single cell calculated on 10 000 events for each samples repeated in triplicates. Dunnett's test: $^{***}p < 0.001$ and $^{*}p < 0.05$, differences between BSA- and Tf-NPs (**a** and **b**) and differences between F98 cells and astrocytes (**c**).

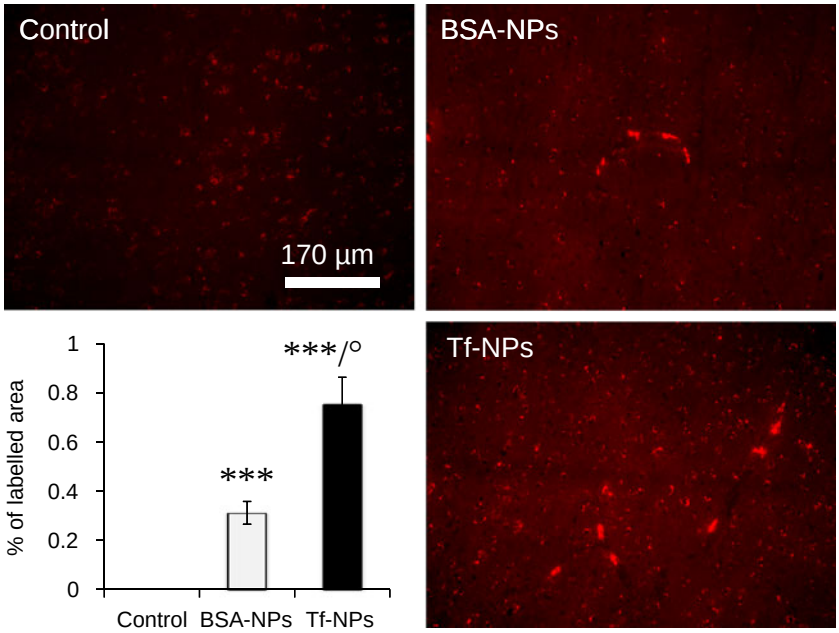


**Fig. 6** Brain accumulation of DiI after i.v injections of DiI-NPs in healthy animals. Evaluation of DiI fluorescence within the brain was made through image software analysis combined with fluorescent microscopy at 2 h after i.v. injection. Representative images are shown of the observations made in the different situations in cortex (Bar: 170 $\mu$m). Control represented background staining in the absence of DiI-NP injections. Note the longitudinal shape of labeled structures. The bar chart shows semi-quantitative analysis of the percentage of the total area that was DiI-labeled. Note that loading NPs with Tf (Tf-NPs) gave a two-fold increase compared with BSA-NPs for DiI accumulation within the cortex. 24 h data after injection gave similar pattern of staining and are thus not included. Dunnett's test: comparison to control (**$p < 0.01$; *$p < 0.05$); comparison between BSA-NPs and Tf-NPs (°$p < 0.05$).

dependent mechanisms as evidenced by strong inhibitory effect of caveolae- (MBC and nystatin) and clathrin-pathway inhibitors (Chlorpromazine and potassium depletion) on their internalization. In contrast, BSA-NPs do not appear to use the caveolae-pathways and displayed a dependency to macropinocytosis (DMA). These results strengthen the point that the

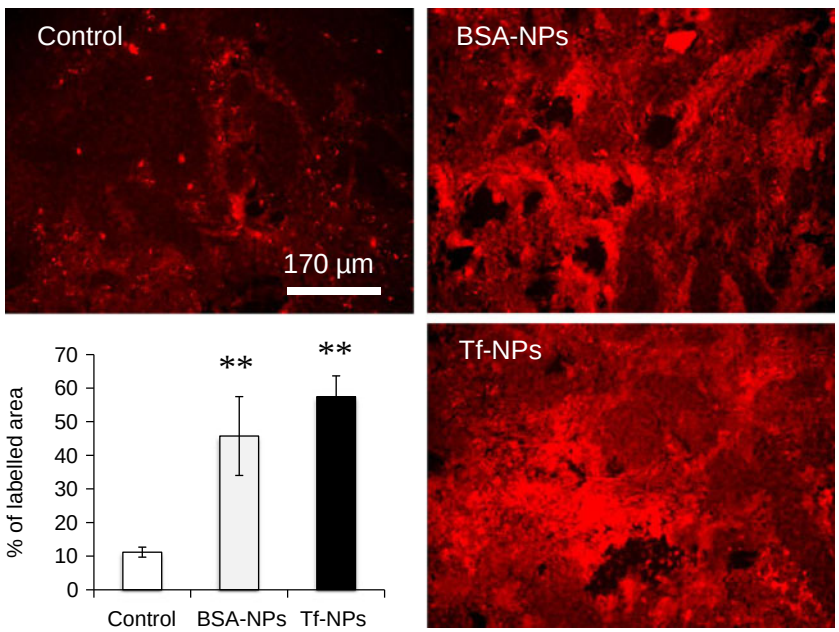


**Fig. 7** Brain accumulation of DiI after i.v. injections of DiI-NPs in orthotopic F98 tumor bearing rats. Evaluation of DiI fluorescence within the brain was made through image software analysis combined with fluorescence microscopy at 24 h after i.v. injection. Representative images of the observations made within the tumor are shown (Bar: 170 $\mu$m). Note the high fluorescence obtained with BSA- and Tf-NPs when compared to tumor auto-fluorescence in the control situation. The bar chart shows semi-quantitative analysis of the percentage of the total area that was DiI-labeled. Dunnett's test: comparison to control (**$p < 0.01$).

specificity of the protein coating implies different mechanisms of endocytosis.

The results presented in Fig. 5a demonstrate a linear dose–response uptake for Blank- and Tf-NPs in glioma cells, while a plateau was observed for BSA-NPs. Higher uptake of Tf-NPs was observed compared to BSA-NPs used as control. Similar data were obtained in astrocytes while Tf-NPs reached a saturation level at 100 μg/mL (Fig. 5b). These observations could be explained by the over expression of the TfR by F98 cells when compared with astrocytes as assessed by OX26 immunostaining (Fig. 5c) and possible distinct TfR recycling at the plasma membrane within the two cell types (67,68).

### Effect of Protein Adsorption on the Ability of NPs to Reach the Brain

Brain accumulation of the different NP formulations was studied after i.v. injections of DiI-labeled BSA- and Tf-NPs in two situations: firstly in healthy animals and secondly in orthotopic F98 tumor-bearing rats at day 19 after tumor cell implantation, when tumors were largely established and clearly detectable through MRI. Evaluation of DiI fluorescence within the brain was made through image software analysis combined with fluorescent microscopy (see Materials and Methods section) at 2 and 24 h after i.v. injection for healthy animals and 24 h for brain tumor accumulation. Figure 6 shows DiI accumulation in cortex of healthy rats. Loading NPs with Tf gave a two-fold increase compared with BSA-NPs. On the structural level, brain areas that were stained with DiI were always longitudinal in shape, thus suggesting that NP were partially located in blood microvessels. Taken together, these data demonstrate that improvement of brain accumulation of nanocarriers through active targeting is more effective with Tf-NPs than BSA-NPs.

In the tumor-bearing animals (Fig. 7), an improvement of accumulation of DiI within the brain was observed when compared with the healthy animals, with the two NP formulations leading to a similar pattern of DiI labeled tumor areas. This observation emphasized that passive accumulation of NPs is possible at this stage of F98 tumor evolution, likely due to disruption of the blood–brain barrier (69). Thus, in established brain tumors, no singular brain targeting of the BSA- or Tf-NPs was observed, which imply that specificity would repose on internalization within tumor cells, which is also a prerequisite for drug delivery and activity, instead of strengthened tissue accumulation.

## CONCLUSION

In this study we tested the importance of targeting NPs to the brain using Tf as a targeting moiety. Protein coating improved NP stability and slightly modified NPs' size and zeta potential and improved their stability under storage. *In vivo* we observed that protein coating highly increased their plasma retention in mice and rats. Meanwhile, they were not recognized by monocytes. Passive (BSA-NPs) and active targeting (Tf-NPs) was further compared in healthy animals where the BBB was not impaired, thus establishing weak retention of BSA-NPs within the brain parenchyma as compared with Tf-NPs. In contrast, in animals with developed brain tumors both BSA- and Tf-coated nanocarriers were observed in the brain suggesting that the BBB was highly impaired. At the cellular level, the greater uptake of Tf-NPs by glioma cells confirms the interest of specific targeting as already observed with an antibody as targeting moiety (70). The greater uptake by F98 glioma cells of the Tf-NPs suggests interaction between Tf and the overexpressed Tf-receptor at the surface of F98 cell plasma membranes and supports specific glioma cell recognition of Tf-coated NPs. Taken together, these data support the expectation that Tf-NPs as small as 90 nm represent an interesting new nanomedicine to deliver therapeutic molecules to glioma cells in the brain from systemic to locoregional strategies at early and late tumor stages. When loaded with radio-sensitizers, alkylating agents or cell signaling inhibitors, as previously incorporated within PLGA templates (48,71), they may, therefore, improve cellular availability of anticancer drugs and lead to one step forward clinical benefit.

## ACKNOWLEDGMENTS & DISCLOSURES

We would like to thank Pierre Legras from the Service Commun d'Animalerie Hospitalo-Universitaire (SCAHU) d'Angers, france for technical support. Archibald Paillard received a PhD fellowship from Le Comité Départemental de Maine-et-Loire de la Ligue Contre le Cancer. This work was supported by La Ligue Nationale Contre le Cancer through an Equipe Labellisée 2007 grant and by the Cancéropôle Grand-Ouest. We would also like to thank Mike Howsam for careful reading of the manuscript.

## REFERENCES

1. Stupp R, Mason WP, van den Bent MJ, Weller M, Fisher B, Taphoorn MJ, *et al.* Radiotherapy plus concomitant and adjuvant temozolomide for glioblastoma. N Engl J Med. 2005;352(10):987–96.
2. Peer D, Karp JM, Hong S, Farokhzad OC, Margalit R, Langer R. Nanocarriers as an emerging platform for cancer therapy. Nat Nanotechnol. 2007;2(12):751–60.
3. Sells RA, Owen RR, New RR, Gilmore IT. Reduction in toxicity of doxorubicin by liposomal entrapment. Lancet. 1987;2(8559):624–5.
4. Rahman A, Treat J, Roh JK, Potkul LA, Alvord WG, Forst D, *et al.* A phase I clinical trial and pharmacokinetic evaluation of

liposome-encapsulated doxorubicin. J Clin Oncol. 1990;8 (6):1093–100.
5. Cowens JW, Creaven PJ, Greco WR, Brenner DE, Tung Y, Ostro M, *et al.* Initial clinical (phase I) trial of TLC D-99 (doxorubicin encapsulated in liposomes). Cancer Res. 1993;53 (12):2796–802.
6. Gabizon A, Catane R, Uziely B, Kaufman B, Safra T, Cohen R, *et al.* Prolonged circulation time and enhanced accumulation in malignant exudates of doxorubicin encapsulated in polyethyleneglycol coated liposomes. Cancer Res. 1994;54(4):987–92.
7. Storm G, ten Kate MT, Working PK, Bakker-Woudenberg IA. Doxorubicin entrapped in sterically stabilized liposomes: effects on bacterial blood clearance capacity of the mononuclear phagocyte system. Clin Cancer Res. 1998;4(1):111–5.
8. Gref R, Minamitake Y, Peracchia MT, Trubetskoy V, Torchilin V, Langer R. Biodegradable long-circulating polymeric nanospheres. Science. 1994;263(5153):1600–3.
9. Couvreur P, Barratt G, Fattal E, Legrand P, Vauthier C. Nanocapsule technology: a review. Crit Rev Ther Drug Carrier Syst. 2002;19(2):99–134.
10. Muller RH, Keck CM. Challenges and solutions for the delivery of biotech drugs—a review of drug nanocrystal technology and lipid nanoparticles. J Biotechnol. 2004;113(1–3):151–70.
11. Garcion E, Lamprecht A, Heurtault B, Paillard A, Aubert-Pouessel A, Denizot B, *et al.* A new generation of anticancer, drug-loaded, colloidal vectors reverses multidrug resistance in glioma and reduces tumor progression in rats. Mol Cancer Ther. 2006;5(7):1710–22.
12. Lacoeuille F, Garcion E, Benoit JP, Lamprecht A. Lipid nanocapsules for intracellular drug delivery of anticancer drugs. J Nanosci Nanotechno. 2007;7(12):4612–7.
13. Pereira de Oliveira M, Garcion E, Venisse N, Benoit JP, Couet W, Olivier JC. Tissue distribution of indinavir administered as solid lipid nanocapsule formulation in mdr1a (+/+) and mdr1a (−/−) CF-1 mice. Pharm Res. 2005;22(11):1898–905.
14. Allard E, Hindre F, Passirani C, Lemaire L, Lepareur N, Noiret N, *et al.* 188Re-loaded lipid nanocapsules as a promising radiopharmaceutical carrier for internal radiotherapy of malignant gliomas. Eur J Nucl Med Mol Imaging. 2008;35(10):1838–46.
15. Allard E, Passirani C, Garcion E, Pigeon P, Vessieres A, Jaouen G, *et al.* Lipid nanocapsules loaded with an organometallic tamoxifen derivative as a novel drug-carrier system for experimental malignant gliomas. J Control Release. 2008;130(2):146–53.
16. Rapoport NY, Kennedy AM, Shea JE, Scaife CL, Nam KH. Controlled and targeted tumor chemotherapy by ultrasound-activated nanoemulsions/microbubbles. J Control Release. 2009;138(3):268–76.
17. Paillard A, Passirani C, Saulnier P, Kroubi M, Garcion E, Benoit JP, *et al.* Positively-charged, porous, polysaccharide nanoparticles loaded with anionic molecules behave as 'stealth' cationic nanocarriers. Pharm Res. 2010;27(1):126–33.
18. Roger E, Lagarce F, Garcion E, Benoit JP. Lipid nanocarriers improve paclitaxel transport throughout human intestinal epithelial cells by using vesicle-mediated transcytosis. J Control Release. 2009;140(2):174–81.
19. Roger E, Lagarce F, Garcion E, Benoit JP. Reciprocal competition between lipid nanocapsules and P-gp for paclitaxel transport across Caco-2 cells. Eur J Pharm Sci. 2010;40(5):422–9.
20. Lemarchand C, Gref R, Passirani C, Garcion E, Petri B, Muller R, *et al.* Influence of polysaccharide coating on the interactions of nanoparticles with biological systems. Biomaterials. 2006;27 (1):108–18.
21. Beduneau A, Saulnier P, Anton N, Hindre F, Passirani C, Rajerison H, *et al.* Pegylated nanocapsules produced by an organic solvent-free method: Evaluation of their stealth properties. Pharm Res. 2006;23(9):2190–9.
22. Vinchon-Petit S, Jarnet D, Paillard A, Benoit JP, Garcion E, Menei P. *In vivo* evaluation of intracellular drug-nanocarriers infused into intracranial tumours by convection-enhanced delivery: distribution and radiosensitisation efficacy. J Neurooncol. 2010;97(2):195–205.
23. Paillard A, Hindre F, Vignes-Colombeix C, Benoit JP, Garcion E. The importance of endo-lysosomal escape with lipid nanocapsules for drug subcellular bioavailability. Biomaterials. 2010;31 (29):7542–54.
24. Weyland M, Manero F, Paillard A, Gree D, Viault G, Jarnet D, et al. Mitochondrial targeting by use of lipid nanocapsules loaded with SV30, an analogue of the small-molecule Bcl-2 inhibitor HA14-1. J Control Release 2011.
25. Faraji AH, Wipf P. Nanoparticles in cellular drug delivery. Bioorg Med Chem. 2009;17(8):2950–62.
26. Moghimi SM, Hunter AC, Murray JC. Nanomedicine: current status and future prospects. FASEB J. 2005;19(3):311–30.
27. Panyam J, Labhasetwar V. Biodegradable nanoparticles for drug and gene delivery to cells and tissue. Adv Drug Deliv Rev. 2003;55(3):329–47.
28. Tosi G, Costantino L, Rivasi F, Ruozi B, Leo E, Vergoni AV, *et al.* Targeting the central nervous system: *in vivo* experiments with peptide-derivatized nanoparticles loaded with Loperamide and Rhodamine-123. J Control Release. 2007;122(1):1–9.
29. Fenart L, Casanova A, Dehouck B, Duhem C, Slupek S, Cecchelli R, *et al.* Evaluation of effect of charge and lipid coating on ability of 60-nm nanoparticles to cross an *in vitro* model of the blood–brain barrier. J Pharmacol Exp Ther. 1999;291(3):1017–22.
30. Jallouli Y, Paillard A, Chang J, Sevin E, Betbeder D. Influence of surface charge and inner composition of porous nanoparticles to cross blood–brain barrier *in vitro*. Int J Pharm. 2007;344(1–2):103–9.
31. Blasi P, Giovagnoli S, Schoubben A, Ricci M, Rossi C. Solid lipid nanoparticles for targeted brain drug delivery. Adv Drug Deliv Rev. 2007;59(6):454–77.
32. Kim HR, Andrieux K, Gil S, Taverna M, Chacun H, Desmaele D, *et al.* Translocation of poly(ethylene glycol-co-hexadecyl) cyanoacrylate nanoparticles into rat brain endothelial cells: role of apolipoproteins in receptor-mediated endocytosis. Biomacromolecules. 2007;8(3):793–9.
33. Kreuter J, Ramge P, Petrov V, Hamm S, Gelperina SE, Engelhardt B, *et al.* Direct evidence that polysorbate-80-coated poly(butylcyanoacrylate) nanoparticles deliver drugs to the CNS via specific mechanisms requiring prior binding of drug to the nanoparticles. Pharm Res. 2003;20(3):409–16.
34. Dehouck B, Fenart L, Dehouck MP, Pierce A, Torpier G, Cecchelli R. A new function for the LDL receptor: transcytosis of LDL across the blood–brain barrier. J Cell Biol. 1997;138 (4):877–89.
35. Duffy KR, Pardridge WM. Blood–brain barrier transcytosis of insulin in developing rabbits. Brain Res. 1987;420(1):32–8.
36. Descamps L, Dehouck MP, Torpier G, Cecchelli R. Receptor-mediated transcytosis of transferrin through blood–brain barrier endothelial cells. Am J Physiol. 1996;270(4 Pt 2):H1149–58.
37. Qian ZM, Li H, Sun H, Ho K. Targeted drug delivery via the transferrin receptor-mediated endocytosis pathway. Pharmacol Rev. 2002;54(4):561–87.
38. Li Y, Ogris M, Wagner E, Pelisek J, Ruffer M. Nanoparticles bearing polyethyleneglycol-coupled transferrin as gene carriers: preparation and *in vitro* evaluation. Int J Pharm. 2003;259(1–2):93–101.
39. Pan X, Guan J, Yoo JW, Epstein AJ, Lee LJ, Lee RJ. Cationic lipid-coated magnetic nanoparticles associated with transferrin for gene delivery. Int J Pharm. 2008;358(1–2):263–70.

40. Sahoo SK, Labhasetwar V. Enhanced antiproliferative activity of transferrin-conjugated paclitaxel-loaded nanoparticles is mediated via sustained intracellular drug retention. Mol Pharm. 2005;2 (5):373–83.
41. Abela RA, Qian J, Xu L, Lawrence TS, Zhang M. Radiation improves gene delivery by a novel transferrin-lipoplex nanoparticle selectively in cancer cells. Cancer Gene Ther. 2008;15(8):496–507.
42. Zhang X, Koh CG, Yu B, Liu S, Piao L, Marcucci G, *et al.* Transferrin receptor targeted lipopolyplexes for delivery of antisense oligonucleotide g3139 in a murine k562 xenograft model. Pharm Res. 2009;26(6):1516–24.
43. Bellocq NC, Pun SH, Jensen GS, Davis ME. Transferrin-containing, cyclodextrin polymer-based particles for tumor-targeted gene delivery. Bioconjug Chem. 2003;14(6):1122–32.
44. Li JL, Wang L, Liu XY, Zhang ZP, Guo HC, Liu WM, *et al.* In vitro cancer cell imaging and therapy using transferrin-conjugated gold nanoparticles. Cancer Lett. 2009;274(2):319–26.
45. Beduneau A, Saulnier P, Hindre F, Clavreul A, Leroux JC, Benoit JP. Design of targeted lipid nanocapsules by conjugation of whole antibodies and antibody Fab' fragments. Biomaterials. 2007;28 (33):4978–90.
46. Dechy-Cabaret O, Martin-Vaca B, Bourissou D. Controlled ring-opening polymerization of lactide and glycolide. Chem Rev. 2004;104(12):6147–76.
47. Chang J, Jallouli Y, Kroubi M, Yuan XB, Feng W, Kang CS, *et al.* Characterization of endocytosis of transferrin-coated PLGA nanoparticles by the blood–brain barrier. Int J Pharm. 2009;379 (2):285–92.
48. Jain A, Chasoo G, Singh SK, Saxena AK, Jain SK. Transferrin-appended PEGylated nanoparticles for temozolomide delivery to brain: *in vitro* characterisation. J Microencapsul. 2011;28(1):21–8.
49. Shah N, Chaudhari K, Dantuluri P, Murthy RS, Das S. Paclitaxel-loaded PLGA nanoparticles surface modified with transferrin and Pluronic((R))P85, an *in vitro* cell line and *in vivo* biodistribution studies on rat model. J Drug Target. 2009;17 (7):533–42.
50. Gan CW, Feng SS. Transferrin-conjugated nanoparticles of poly (lactide)-D-alpha-tocopheryl polyethylene glycol succinate diblock copolymer for targeted drug delivery across the blood–brain barrier. Biomaterials. 2010;31(30):7748–57.
51. Xu F, Lu W, Wu H, Fan L, Gao X, Jiang X. Brain delivery and systemic effect of cationic albumin conjugated PLGA nanoparticles. J Drug Target. 2009;17(6):423–34.
52. Ruben GC, Wang JZ, Iqbal K, Grundke-Iqbal I. Paired helical filaments (PHFs) are a family of single filament structures with a common helical turn period: negatively stained PHF imaged by TEM and measured before and after sonication, deglycosylation, and dephosphorylation. Microsc Res Tech. 2005;67(3–4):175–95.
53. Tsuchiya S, Kobayashi Y, Goto Y, Okumura H, Nakae S, Konno T, *et al.* Induction of maturation in cultured human monocytic leukemia cells by a phorbol diester. Cancer Res. 1982;42(4):1530–6.
54. McCarthy KD, de Vellis J. Preparation of separate astroglial and oligodendroglial cell cultures from rat cerebral tissue. J Cell Biol. 1980;85(3):890–902.
55. Johannes L, Lamaze C. Clathrin-dependent or not: is it still the question? Traffic. 2002;3(7):443–51.
56. Rodal SK, Skretting G, Garred O, Vilhardt F, van Deurs B, Sandvig K. Extraction of cholesterol with methyl-beta-cyclodextrin perturbs formation of clathrin-coated endocytic vesicles. Mol Biol Cell. 1999;10(4):961–74.
57. Larkin JM, Brown MS, Goldstein JL, Anderson RG. Depletion of intracellular potassium arrests coated pit formation and receptor-mediated endocytosis in fibroblasts. Cell. 1983;33(1):273–85.
58. Liu NQ, Lossinsky AS, Popik W, Li X, Gujuluva C, Kriederman B, *et al.* Human immunodeficiency virus type 1 enters brain microvascular endothelia by macropinocytosis dependent on lipid rafts and the mitogen-activated protein kinase signaling pathway. J Virol. 2002;76(13):6689–700.
59. Jain RA. The manufacturing techniques of various drug loaded biodegradable poly(lactide-co-glycolide) (PLGA) devices. Biomaterials. 2000;21(23):2475–90.
60. Klibanov AL, Maruyama K, Torchilin VP, Huang L. Amphipathic polyethyleneglycols effectively prolong the circulation time of liposomes. FEBS Lett. 1990;268(1):235–7.
61. Kreuter J. Drug targeting with nanoparticles. Eur J Drug Metab Pharmacokinet. 1994;19(3):253–6.
62. Vonarbourg A, Passirani C, Saulnier P, Benoit JP. Parameters influencing the stealthiness of colloidal drug delivery systems. Biomaterials. 2006;27(24):4356–73.
63. Daigneault M, Preston JA, Marriott HM, Whyte MK, Dockrell DH. The identification of markers of macrophage differentiation in PMA-stimulated THP-1 cells and monocyte-derived macrophages. PLoS One. 2010;5(1):e8668.
64. Hirata T, Bitterman PB, Mornex JF, Crystal RG. Expression of the transferrin receptor gene during the process of mononuclear phagocyte maturation. J Immunol. 1986;136(4):1339–45.
65. Matveev S, van der Westhuyzen DR, Smart EJ. Co-expression of scavenger receptor-BI and caveolin-1 is associated with enhanced selective cholesteryl ester uptake in THP-1 macrophages. J Lipid Res. 1999;40(9):1647–54.
66. Liu AP, Aguet F, Danuser G, Schmid SL. Local clustering of transferrin receptors promotes clathrin-coated pit initiation. J Cell Biol. 2010;191(7):1381–93.
67. Davis RJ, Corvera S, Czech MP. Insulin stimulates cellular iron uptake and causes the redistribution of intracellular transferrin receptors to the plasma membrane. J Biol Chem. 1986;261 (19):8708–11.
68. Galvez T, Teruel MN, Heo WD, Jones JT, Kim ML, Liou J, *et al.* siRNA screen of the human signaling proteome identifies the PtdIns(3,4,5)P3-mTOR signaling pathway as a primary regulator of transferrin uptake. Genome Biol. 2007;8(7):R142.
69. Schneider SW, Ludwig T, Tatenhorst L, Braune S, Oberleithner H, Senner V, *et al.* Glioblastoma cells release factors that disrupt blood–brain barrier features. Acta Neuropathol. 2004;107(3):272–6.
70. Kirpotin DB, Drummond DC, Shao Y, Shalaby MR, Hong K, Nielsen UB, *et al.* Antibody targeting of long-circulating lipidic nanoparticles does not increase tumor localization but does increase internalization in animal models. Cancer Res. 2006;66 (13):6732–40.
71. Acharya S, Sahoo SK. PLGA nanoparticles containing various anticancer agents and tumour delivery by EPR effect. Adv Drug Deliv Rev. 2011;63(3):170–83.